Available online at www.sciencedirect.com
SCIENCE DIRECT®
Journal of Sound and Vibration 279 (2005) 201–215
JOURNAL OF SOUND AND VIBRATION
www.elsevier.com/locate/jsvi

Effect of spring non-linearity on dynamic stability of a controlled maglev vehicle and its guideway system

Xiao Jing Zheng, Jian Jun Wu*, You-He Zhou

Department of Mechanics, Lanzhou University, Lanzhou, Gansu 730000, People's Republic of China

Received 1 April 2003; accepted 31 October 2003

Abstract

The non-linear effect of a spring on the dynamic characteristics of a magnetically levitated (or maglev) vehicle and its guideway system is numerically studied in this paper. A simplified theoretical model of a maglev vehicle with heavy and forward motions on flexible guideways is suggested to study the coupling among the motions of vehicle, the vibration of guideways, and the control system of the electromagnetic suspension. The stable regions and/or the attracting regions of the attractor of the controlled system either with a non-linear spring or with a linear spring are obtained. It is found that the stable region is strongly dependent upon the non-linear terms of the spring, the forward velocity of the vehicle, and the control parameters. Finally, the chaotic response of the system with a non-linear spring is presented.

1. Introduction

As a new kind of transportation means, the magnetically levitated (maglev) vehicles moving on guideways are found to have better behavior than conventional ground transports, including higher speed, less friction, and lower noise. It is the high speed with potential safety problems that has attracted much attention of researchers. At present, there are mainly two types of maglev vehicles. One is referred to as the electromagnetic system (EMS) whose maglev force is an attraction and is generated by normal electromagnets, while the other is called as the electrodynamic system (EDS) whose maglev force is a repellent one and is induced by superconductors. The equilibrium position(s) of an EMS maglev vehicle is inherently unstable if no force from a feedback control system is applied to the suspended vehicle [1]. Even though we apply the feedback control to the EMS maglev vehicle/guideway coupling system, it can still be

*Corresponding author. Tel.: +86-931-8913912; fax: +86-931-8913554.
E-mail address: wujjun@lzu.edu.cn (J.J. Wu).

0022-460X/$ - see front matter © 2003 Elsevier Ltd. All rights reserved.
doi:10.1016/j.jsv.2003.10.025

unstable when the control parameters are given improperly. Thus, research on the dynamic behavior and stability of the EMS maglev vehicle-guideway-control system with high-speed motion becomes one of the key problems in the safe design of the system.

By using a simplified first order model of the suspended body on a guideway, Chu and Moon [2] conducted an experiment and theoretical analysis to show the instability of the maglev control system. Zhou and Zheng [3] discussed the stable regions of control parameters for a linear maglev system of Moon's model [1]. Takashi and Yoshihisa [4] observed chaotical phenomenon of the magnetic suspension system with linear induction motors.

Moon [1] is the first one to study the control behavior of the vehicle modelled by a lumped mass with a fixed linear spring. Cai et al. [5,6] simulated the dynamic responses of a second order suspended vehicle/guideway system under a concentrated load and a distributed load moving on an elastic beam simply supported at the ends. Cai and Chen [7] numerically studied the dynamic behavior of the moving vehicle and vibration of the guideways with three-degree-of-freedoms (d.o.f.'s) and 5 d.o.f.'s models. Recently, Zheng et al. [8] discussed the stable and dynamic properties of the system coupled with the vehicle movements, guideway vibration, and control sub-system on the basis of a second order suspension body with 5 d.o.f.'s. It should be noted that the springs in the models mentioned above were all considered as linear ones. In practice, however, the spring is non-linear such as the air spring which is usually used in maglev vehicle system. Therefore, it is necessary to investigate the effects of the non-linear spring on the dynamic behavior of such systems.

In this paper, a simplified second order model of a maglev vehicle with a control system moving on a flexible guideway is suggested to investigate the dynamic stability of a maglev system. The coupling among the vehicle movements, guideway vibrations, and control system is taken into account in the theoretical analysis. The control system consists of an electric circuit to generate an electromagnetic force applied to the primary body, and an air spring, either linear or non-linear, connecting the primary and the second suspension bodies. The guideway is simplified as an elastic beam with simply supported ends. The theoretical model suggested here is presented in Section 2. Section 3 exhibits the governing equations in state space when the method of modal expansion is used to obtain the dynamic response of guideway vibration. The Runge–Kutta–Merson method [9] is used to search for the attraction region of stable control, and chaotic response in Section 4. Numerical results to show the effect of a non-linear spring on the dynamic characteristics are shown in Section 5. Finally, Section 6 concludes the paper.

2. Theoretical model

For the simplicity, here, we will focus our attention on the control stability of vertical/or heavy motion of a maglev vehicle with one lump and one carriage which are forwardly moving on a guideway with transverse vibration in vertical direction.

Fig. 1 shows a schematic drawing of the maglev/guideway system. The "magnetic wheel", called the primary suspension body, is suspended by an electromagnetic force generated by a magnetic induction system between the suspended body and the guideway. The bogie with a carriage body, called the secondary suspension body, is supported by one linear or non-linear spring and one damper connected to the primary suspension body.

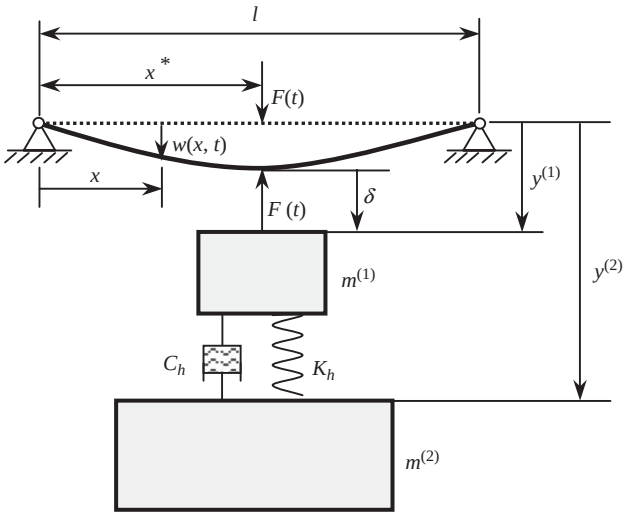

Fig. 1. The schematic drawing of a simplified model to a two order suspension maglev vehicle/guideway system with a control of electromagnetic force $F(t)$.

In the following, we denote $F_1(t)$ the electromagnetic force; $m^{(1)}$ and $m^{(2)}$ the mass of the primary and secondary bodies, respectively; b the effective length and A_0 the cross-sectional area of the "magnetic wheel", respectively; $y^{(1)}$ and $y^{(2)}$ the vertical displacements of the primary and the secondary suspension bodies, respectively. The reaction force in the air spring and the damper, dependent on the vertical displacements $y^{(1)}$ and $y^{(2)}$, is represented by $F_2(t)$. The flexible guideway is treated as an elastic beam of the span length l, the mass density ρ, the damping coefficient C_g and the flexural rigidity EJ. Let $w(x,t)$ be the transverse deflection in vertical direction, where x is a position co-ordinate along the direction of forward motion and t is a time variable. The electromagnetic circuit has N-turns of coil with electric resistance R. The magnetic gap $\delta(t) = y^{(1)}(t) - w^*(t)$, where $w^*(t) = w(x^*, t)$ is the deflection of the guideway at the position of vehicle $x = x^*(t)$.

2.1. Equations for electromagnetic circuit of control system

Assume that the effective magnetic reluctance in the circuit between the "magnetic wheel" and the guideway be $R^*(t)$. Denote the total control current as $I(t)$ applied on the electromagnetic circuit and δ_0 a control goal which is the desired gap between the primary suspension body and the deflected guideway. We can write [3]

$$I(t) = I_0 + i(t), \quad R^*(t) = R_0^* + r^* s(t), \tag{1}$$

where I_0 is a bias current related to the control goal δ_0, and $i(t)$ represents the dynamic part of the control current, R_0^* is the effective reluctance when $\delta = \delta_0$, $r^* = 2/(\mu_0 A_0)$, μ_0 is magnetic permeability of vacuum ($4\pi \times 10^{-7}$ H/m), and $s(t)$ is a suspension disturbance from the control goal, i.e.,

$$s(t) = \delta(t) - \delta_0 = y^{(1)}(t) - w^*(t) - \delta_0. \tag{2}$$

For the dynamic part of the control voltage, $V_c(t)$, applied to the electromagnetic system, we take the following control law:

$$V_c = G_1 s(t) + G_2 \dot{s}(t), \tag{3}$$

where G_1 and G_2 are the control gains. From the theory of electromagnetic circuits, we can write [1]

$$\begin{aligned} N^2 \frac{\mathrm{d}}{\mathrm{d}t}\left[\frac{i(t)}{R^*(t)}\right] &= -RI(t) + V_0 + V_c \\ &= -Ri(t) + G_1(y^{(1)} - w^* - \delta_0) + G_2(\dot{y}^{(1)} - \dot{w}^*), \end{aligned} \tag{4}$$

where $V_0 = I_0 R$ is the bias control voltage when $\delta = \delta_0$. Then the control electromagnetic force $F_1(t)$ is given by [1]

$$F_1(t) = \frac{N^2}{\mu_0 A_0} \frac{I^2(t)}{[R^*(t)]^2}. \tag{5}$$

2.2. Equations for suspended bodies

The static equilibrium of the suspended bodies leads to

$$(m^{(1)} + m^{(2)})g = \frac{N^2}{\mu_0 A_0} \frac{I_0^2}{R_0^{*2}}, \tag{6}$$

where g is the acceleration of gravity. Consider a non-linear relation of an air spring [10]

$$F_2^{(1)}(t) = K_h(y^{(2)} - y^{(1)})[K_a(y^{(2)} - y^{(1)})^2 - 1][K_b(y^{(2)} - y^{(1)})^2 - K_c], \tag{7}$$

in which K_a, K_b and K_c are the constants of non-linear part of the spring, and K_h represents the coefficient of rigidity of linear part of the spring. When $K_a = 0$, $K_b = 0$ and $K_c = 1$, we get the linear relation of the spring,

$$F_2^{(1)}(t) = K_h(y^{(2)} - y^{(1)}). \tag{8}$$

For the damper, we take the linear relation of the form

$$F_2^{(2)}(t) = C_h(\dot{y}^{(2)} - \dot{y}^{(1)}), \tag{9}$$

where C_h is the damping coefficient of the damper. Adding Eqs. (7) or (8) and Eq. (9), we get

$$F_2(t) = F_2^{(1)}(t) + F_2^{(2)}(t). \tag{10}$$

By the second Newton's law, we can write the equations of motion in the vertical direction for the primary and secondary suspension bodies

$$m^{(1)}\ddot{y}^{(1)} = m^{(1)}g - F_1(t) + F_2(t), \tag{11}$$

$$m^{(2)}\ddot{y}^{(2)} = m^{(2)}g - F_2(t). \tag{12}$$

2.3. Dynamic equation for guideway deflection

According to the theory of Bernoulli–Euler beams, the dynamic equation for the deflection of guideways in y direction can be expressed as

$$EJ\frac{\partial^4 w}{\partial x^4}+C_g\frac{\partial w}{\partial t}+\rho\frac{\partial^2 w}{\partial t^2}=\frac{N^2}{\mu_0 A_0}\frac{I^2(t)}{[R^*(t)]^2}\eta(x), \tag{13}$$

where

$$\eta(x)=\begin{cases}1, & vt-\dfrac{b}{2}\leqslant x\leqslant vt+\dfrac{b}{2}\\ 0 & \text{else}\end{cases} \tag{14}$$

and v denotes the speed of vehicle of forward movement in x direction.

Eqs. (4) and (11)–(13) constitute the basic governing equations of the simplified model of the maglev vehicle/guideway system shown in Fig. 1. These equations are coupled non-linearly.

3. Modal expansion method and dynamic equations in state space

We introduce the following dimensionless quantities:

$$\begin{aligned}
&\bar{y}^{(1)}=\frac{y^{(1)}}{l},\quad \bar{y}^{(2)}=\frac{y^{(2)}}{l},\quad \bar{i}=\frac{i}{I_0},\quad \bar{t}=\frac{tv}{l},\quad \bar{x}=\frac{x}{l},\quad \bar{\delta}_0=\frac{\delta_0}{l},\\
&\bar{J}=\frac{J}{l^4},\quad \bar{E}=\frac{El^3}{m^{(1)}v^2},\quad \bar{C}_g=\frac{C_g l}{m^{(1)}v},\quad \bar{\rho}=\frac{\rho l}{m^{(1)}},\quad \bar{g}=\frac{gl}{v^2},\\
&\bar{m}^{(2)}=\frac{m^{(2)}}{m^{(1)}},\quad \bar{b}=\frac{b}{l},\quad \bar{R}_0^*=\frac{R_0^* m^{(1)}v^2}{I_0^2},\quad \bar{r}^*=\frac{r^* m^{(1)}v^2 l}{I_0^2},\quad \bar{R}=\frac{RlI_0^2}{m^{(1)}v^3},\\
&\bar{C}_h=\frac{C_h l}{m^{(1)}v},\quad \bar{K}_h=\frac{K_h l^2}{m^{(1)}v^2},\quad \bar{G}_1=\frac{G_1 l^2 I_0}{m^{(1)}v^3},\quad \bar{G}_2=\frac{G_2 l I_0}{m^{(1)}v^2}.
\end{aligned} \tag{15}$$

Assume that

$$\bar{w}(\bar{x},\bar{t})=\sum_{n=1}^{\infty}Y_n(\bar{t})\Phi_n(\bar{x}), \tag{16}$$

where $Y_n(\bar{t})$ is the nth modal co-ordinate to be determined; $\Phi_n(\bar{x})$ is the pre-chosen modal function of nth order free vibration of the guideway. For a simply supported guideway, the modal functions are

$$\Phi_n(\bar{x})=\sin n\pi\bar{x}. \tag{17}$$

Substituting Eq. (16) into Eq. (13), and applying the Galenkin method, we obtain the dynamic equations for the modal co-ordinates. All the governing equations of the system are now reduced to a set of ordinary differential equations with the unknowns $\bar{y}^{(1)}$, $\bar{y}^{(2)}$, $\bar{i}$, and Y_n $(n=1,2,3,\ldots)$.

In the following discussion, for simplicity, we will drop the bar over dimensionless quantities whenever there is no misunderstanding.

Introducing the following state variables:

$$x_1 = y^{(1)}, \quad x_2 = \dot{y}^{(1)}, \quad x_3 = y^{(2)}, \quad x_4 = \dot{y}^{(2)}, \quad x_5 = i,$$
$$x_{5+(2n-1)} = Y_n, \quad x_{5+2n} = \dot{Y}_n \ (n = 1, 2, 3, \ldots), \tag{18}$$

we can rewrite the dynamic governing equations of the system in the matrix form

$$\dot{\mathbf{X}} = \mathbf{A}\mathbf{X} + \mathbf{B} + \mathbf{C} \equiv \mathbf{F}(\mathbf{x}). \tag{19}$$

Here,

$$\mathbf{X} = [x_1, x_2, x_3, x_4, x_5, \ldots, x_{5+(2n-1)}, x_{5+2n}, \ldots]^{\mathrm{T}} \quad (n = 1, 2, 3, \ldots), \tag{20}$$

where

$$\mathbf{A} = \begin{bmatrix}
0 & 1 & 0 & 0 & 0 & 0 & 0 & 0 & 0 & \cdots \\
-K_h K_c & -C_h & K_h K_c & C_h & 0 & 0 & 0 & 0 & 0 & \cdots \\
0 & 0 & 0 & 1 & 0 & 0 & 0 & 0 & 0 & \cdots \\
\dfrac{K_h K_c}{m^{(2)}} & \dfrac{C_h}{m^{(2)}} & -\dfrac{K_h K_c}{m^{(2)}} & -\dfrac{C_h}{m^{(2)}} & 0 & 0 & 0 & 0 & 0 & \cdots \\
\Gamma_1 G_1 & \Gamma_1 G_2 & 0 & 0 & -\Gamma_1 R & \Delta_{11} & \Delta_{12} & \Delta_{21} & \Delta_{22} & \cdots \\
0 & 0 & 0 & 0 & 0 & 0 & 1 & 0 & 0 & \cdots \\
-\Gamma_3 \Gamma_2 \nu_1 & 0 & 0 & 0 & 2\Gamma_2 \nu_1 & \upsilon_1 - \omega_1^2 & -2\xi_1 \omega_1 & \upsilon_2 & 0 & \cdots \\
0 & 0 & 0 & 0 & 0 & 0 & 0 & 0 & 1 & \cdots \\
-\Gamma_3 \Gamma_2 \nu_2 & 0 & 0 & 0 & 2\Gamma_2 \nu_2 & \upsilon_1 & 0 & \upsilon_2 - \omega_2^2 & -2\xi_2 \omega_2 & \cdots \\
\vdots & \vdots & \vdots & \vdots & \vdots & \vdots & \vdots & \vdots & \vdots & \vdots
\end{bmatrix}, \tag{21}$$

$$\mathbf{B} = \left[0, y_2 - y_1, 0, -\frac{y_2}{m^{(2)}}, y_3, 0, 0, \ldots\right]^{\mathrm{T}}, \tag{22}$$

$$\mathbf{C} = \left[0, g, 0, g, -\Gamma_1 G_1 \delta_0, 0, \Gamma_2 \left(\frac{4r^* A_0}{R_0^*} + 2\right) \nu_1, 0, \Gamma_2 \left(\frac{4r^* A_0}{R_0^*} + 2\right) \nu_2, \ldots\right]^{\mathrm{T}}. \tag{23}$$

Here

$$
\begin{aligned}
y_1 &= (1+m^{(2)})g\frac{(1+x_5)^2}{\left[1+\frac{r^*}{R_0^*}(x_1-w^*-\delta_0)\right]^2},\\
y_2 &= K_hK_aK_b(x_3-x_1)^5 - K_h(K_aK_c+K_b)(x_3-x_1)^3,\\
y_3 &= \frac{r^*}{N^2}(x_1-w^*-\delta_0)[G_1(x_1-w^*-\delta_0)+G_2(x_2-\dot{w}^*)-Rx_5]\\
&\quad + \frac{r^*(x_2-\dot{w}^*)(1+x_5)}{R_0^*+r^*(x_1-w^*-\delta_0)},\\
\Delta_{i1} &= -\Gamma_1(G_1\sin i\pi t + i\pi G_2\cos i\pi t),\\
\Delta_{i2} &= -\Gamma_1 G_2\sin i\pi t, \quad \omega_i = i^2\pi^2\sqrt{EJ/\rho},\\
\Gamma_1 &= \frac{R_0^*}{N^2}, \quad \Gamma_2 = \frac{2(1+m^{(2)})g}{b\rho}, \quad \Gamma_3 = \frac{2(1+m^{(2)})gb}{\pi}, \quad \xi_i = \frac{C_g}{2\rho\omega_i},\\
v_i &= \int_0^1 \eta(x)\sin i\pi t\,\mathrm{d}t = \int_{\max(t-1/2,0)}^{\min(t+1/2,1)} \sin i\pi t\,\mathrm{d}t,\\
\upsilon_i &= \frac{4r^*}{R_0^*}\Gamma_2 v_i\sin i\pi t, \quad (i=1,2,3,\ldots).
\end{aligned}
\tag{24}
$$

When $K_a=0$, $K_b=0$ and $K_c=1$, the dynamic equation (19) describes the system with linear springs.

4. Numerical analysis

In this section, we present numerical algorithms for searching the attraction region in the state space, and the chaotic responses.

4.1. The region of attraction of control goal

The notation $\mathbf{X}(\mathbf{X}_0^*,t)$ is designated a solution of Eq. (19) starting from a pre-given initial condition $\mathbf{X}(t)|_{t=0}=\mathbf{X}_0^*$. Let Ω be the region of attraction of a pre-specified control goal for the system described by $\mathbf{X}_\infty$, and L be a set of all points on its boundary. Then we can say $\mathbf{X}_0^*\in\Omega$, if and only if $\lim_{t\to\infty}\mathbf{X}(\mathbf{X}_0^*,t)=\mathbf{X}_\infty$, i.e., $\lim_{t\to\infty}d(\mathbf{X}(\mathbf{X}_0^*;t),\mathbf{X}_\infty)=0$, in which $d(\cdot,\cdot)$ represents the distance with the Euler's norm. Assume that a point $\mathbf{X}_0^*$ be in the set L, we can express L as

$$
L=\left\{\mathbf{X}_0^*\middle|\lim_{t\to\infty}d(\mathbf{X}(\mathbf{X}_0^*-\varepsilon\mathbf{n};t),\mathbf{X}_\infty)=0,\lim_{t\to\infty}d(\mathbf{X}(\mathbf{X}_0^*+\varepsilon\mathbf{n};t),\mathbf{X}_\infty)\neq 0\right\} \tag{25}
$$

in which ε is arbitrary small quantity, and $\mathbf{n}$ is the normal vector of L, pointing away from Ω. A search algorithm for L is presented next.

Step 1: Choose two initial points **a** and **b**, in the state space. Then we numerically integrate Eq. (19) with **a** and **b** as initial conditions. Observe whether or not the solutions converge to the

control goal. When both are in or not in Ω, we change one of them until one is in Ω and another one is not in Ω. Without losing generality, assume $\mathbf{a}$ in Ω and $\mathbf{b}$ not in Ω. In order to find a point on the boundary L, we take

$$\mathbf{x}_1 = \lambda\mathbf{a} + (1-\lambda)\mathbf{b}, \tag{26}$$

where $0<\lambda<1$ and the value of λ is pre-specified. Next, check whether $\mathbf{x}_1$ is in Ω or not. If $\mathbf{x}_1$ is in Ω, then we take $\mathbf{a}_1 = \mathbf{x}_1$ and $\mathbf{b}_1 = \mathbf{b}$. Otherwise, $\mathbf{a}_1 = \mathbf{a}$ and $\mathbf{b}_1 = \mathbf{x}_1$. Replace $\mathbf{a}$ and $\mathbf{b}$ in Eq. (26) by $\mathbf{a}_1$ and $\mathbf{b}_1$, respectively, and repeat the process. We obtain a set of points with $(\mathbf{a}_j, \mathbf{b}_j)$ $(j = 2, 3, \ldots, m)$ until the following condition:

$$\|\mathbf{b}_m - \mathbf{a}_m\| = \theta^m\|\mathbf{b} - \mathbf{a}\| < \varepsilon_1 \tag{27}$$

is satisfied. Here, $\theta = 1-\lambda$ or λ, and ε_1 is a pre-given precision. Then,

$$\mathbf{X}_0^* = \mathbf{x}_m = \lambda\mathbf{a}_m + (1-\lambda)\mathbf{b}_m \tag{28}$$

is on the boundary L. In the numerical calculations, we take $\lambda = \frac{1}{3}$.

Step 2: After the first point on the boundary L is found, we continue to find its neighboring point on L. Since Ω in general has a high dimension, searching for the boundary L can be computationally intensive. In the following, we focus on the initial conditions of the gap of vehicle motion. In other words, we look at a two-dimensional projection of Ω, which has a one-dimensional boundary. The attraction region and its boundary are dependent upon the parameters of the dynamic system, especially, the control parameters G_1 and G_2.

Let $\mathbf{x}_0^* = (x_{10}^*, x_{20}^*)^{\mathrm{T}}$ be the point found on L. The search for the next point starts from

$$\hat{x}_1^* = x_{10}^* \pm \delta_1, \tag{29}$$

where δ_1 is the given step. We then identify if $(\hat{x}_1^*, x_{20}^*)$ is in Ω or not. Next, we add or subtract δ_2 to the coordinate x_{20}^* until $(\hat{x}_1^*, x_{20}^* \pm \delta_2)$ is opposite to $(\hat{x}_1^*, x_{20}^*)$. At this time, we apply step 1 to find another point on L.

It should be noted that maximum or minimum of x_{10}^* can appear in the curve L. When this happens, we change the operation from '+' to '−', or from '−' to '+' in Eq. (29).

4.2. Chaotic responses

Due to the non-linear factors in the dynamic system, chaotic motions can occur. From the theory of chaos [10], we know that a chaotic motion can be determined by its characteristics including Poincaré-mapping pattern, phase portrait, continuous density of power spectrum, fractal dimension of the chaotic attractor, and positive Lyapunov exponent. We shall consider the power spectrum density and Lyapunov exponents.

4.2.1. Density of power spectrum

Denote a time-response by $x(t)$. Then, its density of power spectrum can be formulated by [11]

$$C(\omega_t) = |\hat{x}(\omega_t)|^2 = \left| \lim_{T\to\infty} \frac{1}{T} \int_0^{\mathrm{T}} x(t) \mathrm{e}^{-\mathrm{i}\omega_t t}\, \mathrm{d}t \right|^2. \tag{30}$$

Here, ω_t indicates the frequency variable. A chaotic motion display the characteristic of continuous broadband function of density of power spectrum with respect to ω_t. Here, we use the fast Fourior transform (FFT) to calculate the density of power spectrum of $x(t)$.

4.2.2. Lyapunuv exponents

Let $\mathbf{X}(t^*) = (x_1(t^*), x_2(t^*), x_3(t^*), \ldots, x_n(t^*))^{\mathrm{T}}$ be a solution of the dynamic differential equation (19) at instant time t^*. Denote

$$D\mathbf{F}(\mathbf{X}(t^*)) = \begin{bmatrix} \dfrac{\partial f_1}{\partial x_1} & \dfrac{\partial f_1}{\partial x_2} & \cdots & \dfrac{\partial f_1}{\partial x_n} \\ \dfrac{\partial f_2}{\partial x_1} & \dfrac{\partial f_2}{\partial x_2} & \cdots & \dfrac{\partial f_2}{\partial x_n} \\ \vdots & \vdots & \cdots & \vdots \\ \dfrac{\partial f_n}{\partial x_1} & \dfrac{\partial f_n}{\partial x_2} & \cdots & \dfrac{\partial f_n}{\partial x_n} \end{bmatrix}_{\mathbf{X}=\mathbf{X}(t^*)}, \tag{31}$$

which is called the fundamental matrix of the differential equations (19). Assume $\mathbf{w}(t)$ be a tangent vector in the solution space of Eq. (19) at point $\mathbf{X}(t^*)$. That is, the tangent vector satisfies the following linear homogenous differential equation:

$$\dot{\mathbf{w}}(t) = D\mathbf{F}(\mathbf{X}(t^*))\mathbf{w}(t), \quad t > t^*. \tag{32}$$

Denote $\mathbf{\Phi}(t, t^*)$ being a matrix composed of fundamental solutions of Eq. (32) with initial condition $\mathbf{\Phi}(t^*, t^*) = \mathbf{I}$ where $\mathbf{I}$ is a unit square matrix of order $n \times n$. If $\mathbf{w}(t^*)/\|\mathbf{w}(t^*)\|$ is a unit vector to Eq. (32) at $t = t^*$, then, the solution of Eq. (32) with this initial condition can be formulated by

$$\mathbf{w}(t, t^*) = \mathbf{\Phi}(t, t^*)\mathbf{w}(t^*)/\|\mathbf{w}(t^*)\|, \tag{33}$$

where $\mathbf{w}(0)$ be an initial disturbance to Eq. (32) at $t^* = 0$. Dividing the time interval $[0, t^*]$ by the nodes $0 = t_0 < t_1 < t_3 < \cdots < t_n = t^*$, by means of the transition matrix of the solution

$$\mathbf{\Phi}_{t_j} = \mathbf{\Phi}(t_j, t_{j-1}), \tag{34}$$

and Eq. (33) at each time step, we can get

$$\begin{aligned} \mathbf{w}(t_n, t_{n-1}) &= \mathbf{\Phi}_{t_n}\mathbf{w}(t_{n-1}, t_{n-2})/\|\mathbf{w}(t_{n-1}, t_{n-2})\| \\ &= \cdots = \mathbf{\Phi}_{t_n}\mathbf{\Phi}_{t_{n-1}}\mathbf{\Phi}_{t_{n-2}}\cdots\mathbf{\Phi}_{t_1}\mathbf{w}(0) \Big/ \left(\prod_{j=0}^{n-1} \|\mathbf{w}(t_j, t_{j-1})\| \right), \end{aligned} \tag{35}$$

in which $\mathbf{w}(0, t_{-1}) = \mathbf{w}(0)$. Hence, we have

$$\hat{\mathbf{w}}(t_n, \mathbf{w}(0)) = \mathbf{\Phi}_{t_n}\mathbf{\Phi}_{t_{n-1}}\mathbf{\Phi}_{t_{n-2}}\cdots\mathbf{\Phi}_{t_1}\mathbf{w}(0) = \mathbf{w}(t_n, t_{n-1}) \prod_{j=0}^{n-1} \|\mathbf{w}(t_j, t_{j-1})\|. \tag{36}$$

The largest Lyapunov exponent [11] is given by

$$\sigma_1 = \lim_{t_n \to \infty} \frac{1}{t_n} \ln \frac{\|\hat{\mathbf{w}}(t_n, \mathbf{w}(0))\|}{\|\mathbf{w}(0)\|}. \tag{37}$$

In practical calculations, the maximum index n of time step is a finite integer, e.g., N. For this case, we have an approximate value of σ_1, denote it by σ_1^N

$$\sigma_1^N = \frac{1}{t_N} \ln \frac{\|\hat{\mathbf{w}}(t_N, \mathbf{w}(0))\|}{\|\mathbf{w}(0)\|}. \tag{38}$$

Substituting Eq. (36) into Eq. (38), we get

$$\sigma_N = \frac{1}{t_N} \sum_{j=1}^{N} \ln\|\mathbf{w}(t_j, t_{j-1})\|. \tag{39}$$

When σ_1^N is convergent as N increases, i.e., the condition

$$\|\sigma_1^{(N+1)} - \sigma_1^{(N)}\| < \varepsilon_2 \tag{40}$$

is satisfied, we get an approximate value of σ_1 of Eq. (37). Here, ε_2 is a pre-given precision.

5. Numerical results and discussions

This section presents numerical results. Table 1 lists geometric and physical parameters used in the numerical simulations.

Fig. 2 exhibits a comparison of dynamic responses of vertical displacement x_1 of the primary suspension body, i.e., "magnetic wheel" in the maglev vehicle system, with linear springs ($K_a = 0,\ K_b = 0,\ K_c = 1$) and non-linear spring ($K_a = 1,\ K_b = 1,\ K_c = 3$) when the vehicle has a forward velocity $v = 100$ m/s, the dynamic control parameters are $G_1 = 0.22$ and $G_2 = 1.84$, and the same initial conditions. For the case of the linear spring, Fig. 2(a) shows a convergent response to the primary suspension body under the control parameters. However, it is found in Fig. 2(b) that the dynamic system becomes unstable when some non-linear terms of the spring are considered. This tells us that there is notable effect of the non-linear terms of spring on the stability of the dynamic control system for some cases of the control parameters.

Fig. 3 shows the change of attraction region of the control goal. In Fig. 3(a), the attraction region of the system with non-linear spring is included in the region of the system with linear spring when the control parameters $G_1 = 0.26$ and $G_2 = 6.22$, that is, the attraction region for the non-linear case is smaller than that for the linear case. When the control parameters $G_1 = 0.26$ and $G_2 = 155.56$, however, the effect of non-linear parts of the spring on the dynamic system is quite different from the former case, which is shown in Fig. 3(b). It is found that there are three subregions denoted by "A", "B" and "C". When an initial state is located in the subregion

Table 1
Geometrical and physical parameters of the maglev vehicle system

ρ	112.5	$m^{(2)}$	2.5	R_0^*	3.2×10^6
EJ	18.7	A_0	4.5×10^{-5}	r^*	2.9×10^6
C_g	2.1×10^{-6}	b	0.2	R	1.5×10^{-6}
δ_0	4.0×10^{-4}	K_h	55.6	N	320
		C_h	20.8		

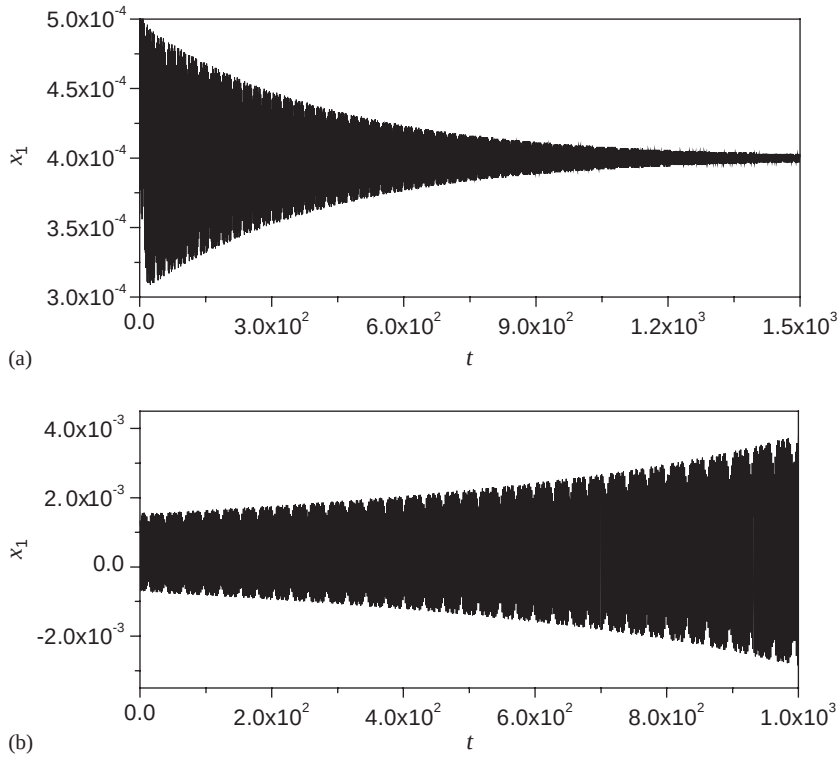

Fig. 2. A comparison of dynamical responses of vertical displacement to the primary suspension of the maglev system with (a) the linear spring and (b) the non-linear spring.

"A", the system under control is stable for the case either linear spring or non-linear spring ($K_a = 1,\ K_b = 1,\ K_c = 3$). In this region, the non-linear part of the spring does not influence the stability of the system. When an initial state is taken in the subregion "B", however, the dynamic control system with the non-linear spring displays stable motion, but the system with linear spring is unstable to the same control goal. In the subregion "C", the system with linear spring is stable but with non-linear spring is unstable. This fact shows that the non-linear part of the spring notably influences the attraction region of the maglev vehicle system.

The attraction region and stability of the maglev control system as a function of the control parameters G_1 and G_2 are plotted in Fig. 4. In Fig. 4(a), (b), the control parameter $G_1 = 0.26$, while G_2 varies. While, Fig. 4(c), (d) shows the attraction regions for the case that $G_2 = 38.88$ when G_1 varies.

It is found that when G_1 increases, the attraction regions for both linear and non-linear spring are shrinking towards the control goal of the system. The numerical simulation shows, however, the suppressing ability to an initial disturbance decreases with increment of G_1. From Fig. 4, we can find the attraction regions of the dynamic system under same control parameters are distinctively different when the connect spring is considered non-linear part from that when it is a linear one. In practice, it is unavoidable that there are some non-linear factors in the spring. In

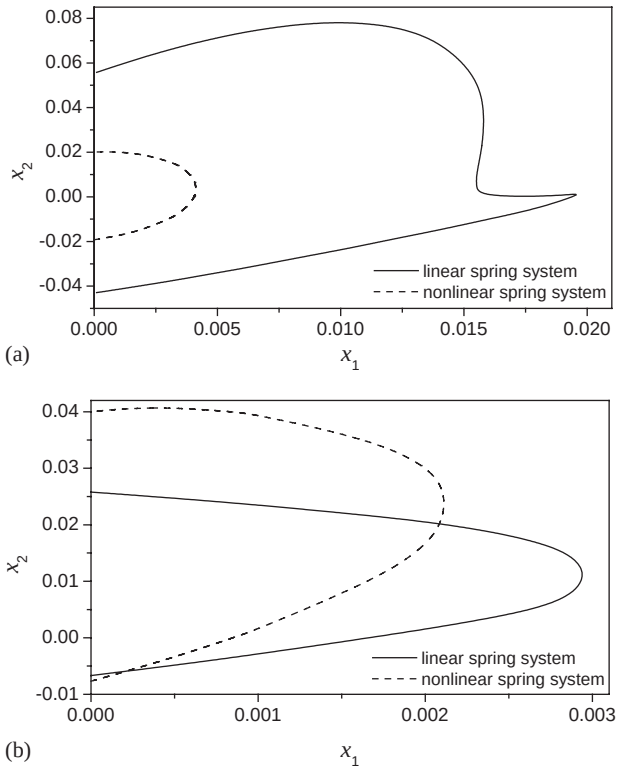

Fig. 3. Comparison of the attraction regions of the asymptotically stable control for the maglev system with the linear and the non-linear springs under two sets of the controlling parameters: (a) $G_1 = 0.26$, $G_2 = 6.22$; (b) $G_1 = 0.26$, $G_2 = 155.56$.

this case, we have to use the theoretic analysis of the model with the non-linear spring to deal with the safety design of high-speed vehicle.

When the control parameters are pre-chosen, e.g., $G_1 = 26.0$ and $G_2 = 217.8$, the attraction region of the system is also related to the forward moving velocity v. Fig. 5 shows the variation of the attraction region to the maglev control system with forward velocity $v = 50$, 100 and 150 m/s. With the increment of the forward speed, the attraction region becomes less generally under a given control. At the same time, there are exceptions when the maglev vehicle system with low speed is unstable but is stable when the maglev control system has high-forward speed.

Finally, we give an example for a non-linear system to show that the maglev control system with the non-linear spring exhibits the chaotic motion. For this purpose, we consider a periodic excitation $f \sin \omega t$ exerted on the maglev vehicle. Fig. 6 shows the time-response of the vertical displacement, $x_1(t)$, its phase portrait in the state space, the Poincaré-mapping pattern, the power spectrum density, and the largest Lyapunov exponent. Here, $f = 0.20$, $\omega = 5.87 \times 10^{-3}$, $G_1 = 3.74 \times 10^{-2}$, $G_2 = 10.16$. It is found from Fig. 6 that the responses all display the characteristic of chaotic motion, i.e., a chaotic attractor because it has a continuous decreasing power spectrum, and a positive Lyapunov exponent. This phenomenon of chaotic motion cannot be found in the maglev vehicle system with a linear spring.

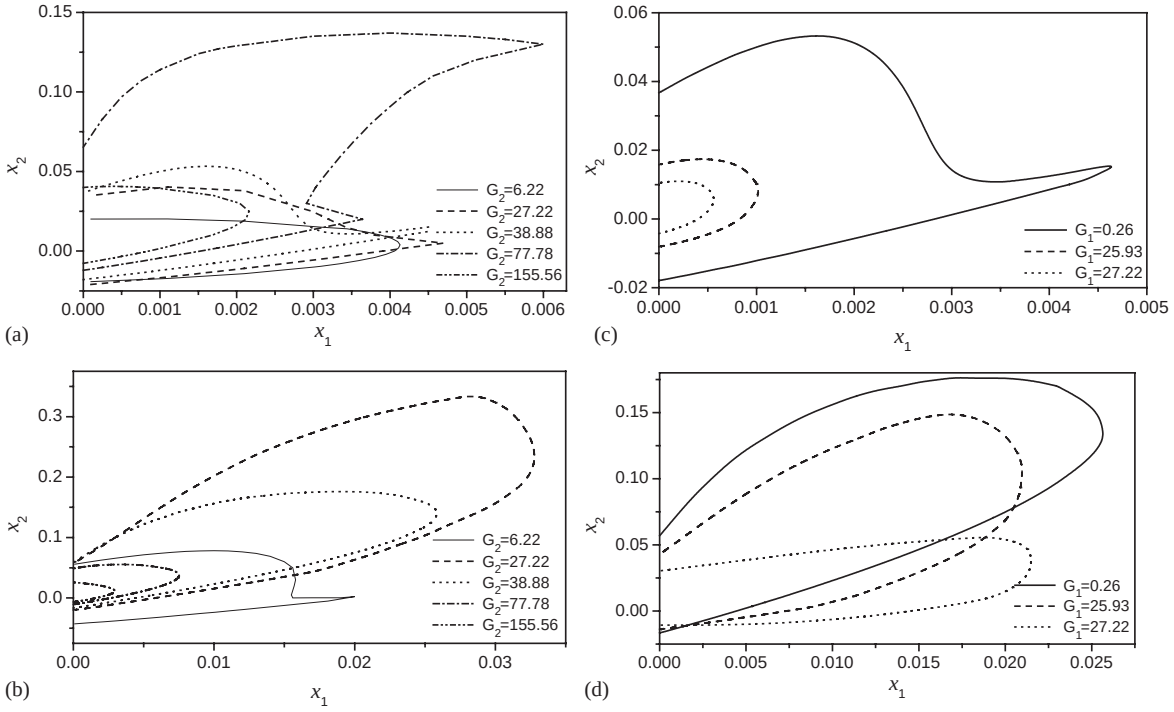

Fig. 4. Dependence of attraction regions of the dynamic control system on the control parameters G_1 and G_2: (a) with the linear springs ($G_1 = 0.26$); (b) with the non-linear springs ($G_1 = 0.26$); (c) with the linear springs ($G_2 = 38.88$); (d) with the non-linear springs ($G_2 = 38.88$).

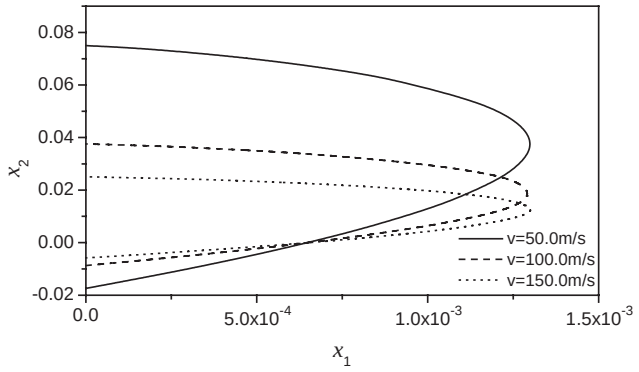

Fig. 5. The influence of the vehicle speed on the attraction region of the maglev vehicle system with non-linear spring under the control parameter $G_1 = 26.0$ and $G_2 = 217.8$.

6. Conclusions

Based on the simplified model of a maglev vehicle/guideway system with a non-linear spring, the numerical simulations are performed on the dynamical stability and the attraction regions. The main conclusions are as follows.

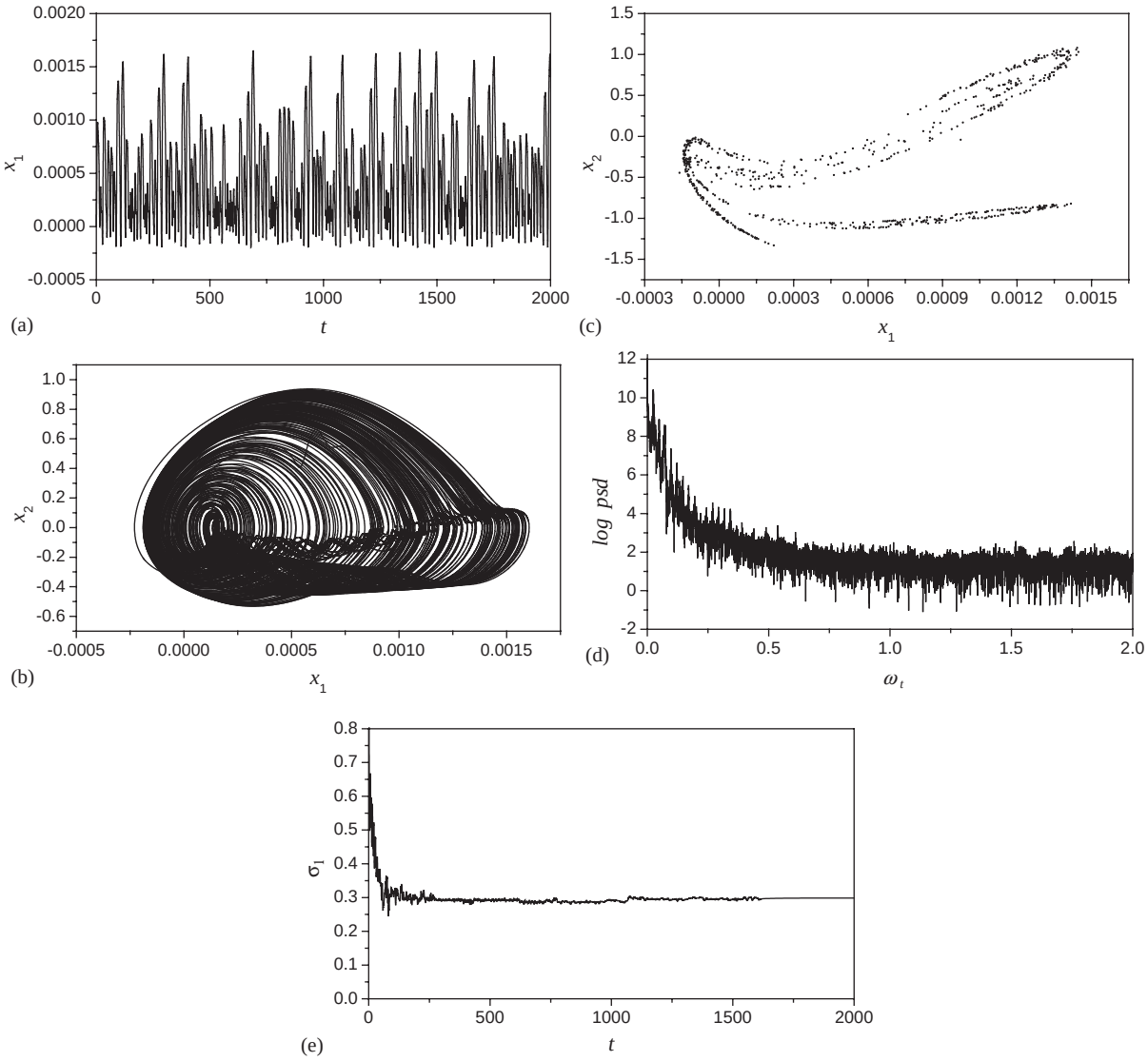

Fig. 6. A chaotic motion of the non-linear spring maglev vehicle system under an external excitation $f = 0.2$, $\omega = 5.87 \times 10^{-3}$, $G_1 = 3.74 \times 10^{-2}$, $G_2 = 10.16$: (a) time-response of vertical displacement; (b) phase portrait; (c) Poincaré map; (d) density of power spectrum; (e) the largest Lyapunov exponent.

(1) The non-linear spring has significant effects on the attraction regions of the dynamic control system as well as the stability of the system.

(2) The attraction regions of the system with a non-linear spring are different from those with a linear spring, and they are affected by the control parameters profoundly. At certain control parameters G_1 and G_2, the attraction region of the system attains to the largest one, no matter for linear or non-linear spring. But with the increment of vehicle speed, the attraction region becomes less and less for the given control parameters.

(3) When the maglev vehicle system under a certain control is subjected to a periodic excitation, the chaotic phenomenon has been found in the system with a non-linear spring. However, no chaos appears in the system with a linear spring.

In reality, the non-linear effect of the spring is unavoidable in the maglev vehicle/guideway control system. Therefore, more researches on the system should be paid on the non-linearity of spring such that the safety design is ensured.

Acknowledgements

This research was supported by the Key Fund of the National Natural Science Foundation (No.10132010), the Excellent Young Teachers Program of MOE, P. R. C.(EYTP), and the Pre-Research fund of Key Basic Researches of the Ministry of Science and Technology of China. The authors sincerely appreciate these supports.

References

[1] F.C. Moon, *Magneto-Solid Mechanics*, Wiley, New York, 1984.
[2] D. Chu, F.C. Moon, Dynamic instabilities in magnetically levitated models, *Journal of Applied Physics* 54 (1983) 1619–1625.
[3] Y.H. Zhou, X.J. Zheng, Dynamic stability of electromagnetic levitation with feedback control, *Journal of Vibration Engineering* 10 (1997) 474–479 (in Chinese).
[4] H. Takashi, H. Yoshihisa, Simulated levitation characteristics of magnetic suspension system by linear induction motor, *International Journal of Applied Electromagnetics in Materials* 3 (1992) 73–85.
[5] Y. Cai, S.S. Chen, D.M. Rote, H.T. Coffey, Vehicle/guideway interaction for high speed vehicles on a flexible guideway, *Journal of Sound and Vibration* 175 (1994) 625–646.
[6] Y. Cai, S.S. Chen, D.M. Rote, H.T. Coffey, Vehicle/guideway dynamic interaction in maglev systems, *Journal of Dynamic Systems, Measurement, and Control, Transaction of ASME* 118 (1996) 526–530.
[7] Y. Cai, S.S. Chen, Numerical analysis for dynamic instability of electrodynamic maglev systems, *Shock and Vibration* 2 (1995) 339–349.
[8] X.J. Zheng, J.J. Wu, Y.H. Zhou, Numerical analyses on dynamic control of five-degree-of-freedom maglev vehicle moving on flexible guideways, *Journal of Sound and Vibration* 235 (2000) 43–61.
[9] M. Kubíček, M. Marek, *Computational Methods in Bifurcation Theory and Dissipative Structures*, Springer, New York, 1983.
[10] F.C. Moon, *Chaotic Vibration*, Wiley, New York, 1987.
[11] F.H. Ling, *Numerical Researches for Nonlinear Dynamic Systems*, Publisher of Shanghai Jiaotong University, Shanghai, 1989 (in Chinese).